

Subsampled directed-percolation models explain scaling relations experimentally observed in the brain

Tawan T. A. Carvalho,¹ Antonio J. Fontenele,¹ Mauricio Girardi-Schappo,^{2,3} Thaís Feliciano,¹ Leandro A. A. Aguiar,⁴ Thais P. L. Silva,¹ Nivaldo A. P. de Vasconcelos,^{1,5,6} Pedro V. Carelli,¹ and Mauro Copelli^{1,*}

¹*Departamento de Física, Universidade Federal de Pernambuco, Recife, PE, 50670-901, Brazil*

²*Physics Department, STEM Complex, University of Ottawa, Ottawa, ON, K1N 6N5, Canada*

³*Departamento de Física, FFCLRP, Universidade de São Paulo, Ribeirão Preto, SP, 14040-901, Brazil*

⁴*Departamento de Ciências Fundamentais e Sociais, Universidade Federal da Paraíba, Areia, PB, 58397-000, Brazil*

⁵*Life and Health Sciences Research Institute (ICVS), School of Medicine, University of Minho, Braga, 4710-057, Portugal*

⁶*ICVS/3Bs - PT Government Associate Laboratory, Braga/Guimarães, Portugal*

(Dated: December 14, 2021)

Recent experimental results on spike avalanches measured in the urethane-anesthetized rat cortex have revealed scaling relations that indicate a phase transition at a specific level of cortical firing rate variability. The scaling relations point to critical exponents whose values differ from those of a branching process, which has been the canonical model employed to understand brain criticality. This suggested that a different model, with a different phase transition, might be required to explain the data. Here we show that this is not necessarily the case. By employing two different models belonging to the same universality class as the branching process (mean-field directed percolation) and treating the simulation data exactly like experimental data, we reproduce most of the experimental results. We find that subsampling the model and adjusting the time bin used to define avalanches (as done with experimental data) are sufficient ingredients to change the apparent exponents of the critical point. Moreover, experimental data is only reproduced within a very narrow range in parameter space around the phase transition.

I. INTRODUCTION

In the first results that fueled the critical brain hypothesis, Beggs and Plenz [1] observed intermittent bursts of local field potentials (LFPs) in *in vitro* multielectrode recordings of cultured slices of the rat brain. Events occurred with a clear separation of time scales, and were named neuronal avalanches.

A neuronal avalanche can be characterized by its size S , which is the total number of events recorded by electrodes between periods of silence, and by its duration T , which is the number of consecutive time bins spanned by an avalanche. Beggs and Plenz found power-law distributions for the sizes of avalanches,

$$P(S) \sim S^{-\tau}, \quad (1)$$

with $\tau \simeq 3/2$, and suggested, based on their data, a power-law distribution of avalanche duration,

$$P(T) \sim T^{-\tau_t}, \quad (2)$$

with $\tau_t = 2$. These scale-invariant distributions were interpreted as a signature that the brain could be operating at criticality – a second-order phase transition [1–4]. In particular, these two critical exponents together are compatible with a branching process at its critical point [5], thus pointing to a phase transition between a so-called

absorbing phase (zero population firing rate) and an active phase (non-zero stationary population firing rate).

Due to its appeal, simplicity and familiarity within the statistical physics community, the critical branching process has become a canonical model for understanding criticality in the brain. In fact, these exponents are compatible with a larger class of models, namely, any model belonging to the mean-field directed percolation (MF-DP) universality class [6]. In the theory of critical phenomena, two models which can be different in their details are said to belong to the same universality class when the critical exponents which characterize their phase transition coincide [7]. In general, probabilistic contagion-like models which have a unique absorbing state (all sites “susceptible” or, in the neuroscience context, all neurons quiescent) and no further symmetries tend to belong to the directed-percolation universality class [8–10]. If the network has topological dimension above 4 (such as random or complete graphs), the model usually belongs to the MF-DP universality class.

More recent experimental results, however, challenged the MF-DP scenario proposed by Beggs and Plenz [1]. For instance, avalanche exponents in ex-vivo recordings of the turtle visual cortex deviated significantly from $\tau = 3/2$ and $\tau_t = 2$ [11]. Discrepancies in exponent values were also observed in spike avalanches of rats under ketamine-xylazine anesthesia [12] and M/EEG avalanches in resting or behaving humans [13, 14], among others.

Furthermore, Touboul and Destexhe [15] argued that the power-law signature alone in the distributions of size

* mauro.copelli@ufpe.br

(Equation 1) and duration (Equation 2) of avalanches is insufficient to claim criticality, since power laws can be observed in non-critical models as well. They suggested that another scaling relation should be tested as a stronger criterion. This was based on the result that at criticality the average avalanche size $\langle S \rangle$ for a given duration T must obey

$$\langle S \rangle \sim T^{\frac{1}{\sigma\nu z}}, \quad (3)$$

where $1/(\sigma\nu z)$ is a combination of critical exponents that at criticality satisfy the so-called crackling noise scaling relation [6, 16, 17]

$$\frac{1}{\sigma\nu z} = \frac{\tau_t - 1}{\tau - 1}. \quad (4)$$

Equation (4) is a stronger criterion for criticality because it is expected not to be satisfied by non-critical models [15]. In the MF-DP case, the avalanche exponents obey $(\tau_t - 1)/(\tau - 1) = 2$ and $1/(\sigma\nu z) = 2$, independently. The absolute difference between the two sides of Equation (4) can even be employed as a metric for the distance to criticality [18], or to identify criticality in more general phase transitions of neuronal networks [19].

Recently, Fontenele et al. [20] investigated cortical spike avalanches of urethane-anesthetized rats using these equations. This experimental setup is known to yield spiking activity which is highly variable, ranging from strongly asynchronous to very synchronous population activity [21]. The synchronicity regimes can be characterized by different ranges of the coefficient of variation (CV) of the instantaneous population firing rate [22], which is used as a proxy to the cortical state, in a time resolution of seconds [23]. By parsing the data according to levels of spiking variability, Fontenele et al. [20] found that the scaling relation in Equation (4) was only satisfied at an intermediate value of CV . They suggested that a critical point is then present in cortical activity away from both the desynchronized and synchronized ends of the spiking variability spectrum. However, the critical exponents were, again, not compatible (within error bars) with MF-DP values: $\langle \tau \rangle \simeq 1.52 \pm 0.09$, $\langle \tau_t \rangle \simeq 1.7 \pm 0.1$ and $\langle 1/(\sigma\nu z) \rangle \simeq 1.28 \pm 0.03$. They interpreted those results as an incompatibility with the theoretical MF-DP scenario [20].

Here we revisit this issue by studying the data produced by two theoretical models in the MF-DP universality class under the same conditions as those of experimental data. Despite the large number of simulated neurons ($\sim 10^5$), we intentionally restrict the theoretical analysis to a small subset of cells ($\sim 10^2$), mimicking the fact that one can only record a few hundred neurons among the millions that comprise the rat's brain – a technique called subsampling. Different groups have shown that subsampling alters the apparent distribution of avalanches [12, 24–29]. We show that combining subsampling with the experimental pipeline reconcile the empirical power-law avalanches with the theoretical MF-DP universality class.

II. METHODS

A. A spiking neuronal network with excitation and inhibition

We use the excitatory/inhibitory network of Girardi-Schappo et al. [30], where each neuron is a stochastic leaky integrate-and-fire unit with discrete time step equal to 1 ms, connected in an all-to-all graph. A binary variable indicates if the neuron fired ($X(t) = 1$) or not ($X(t) = 0$). The membrane potential of each cell i in either the excitatory (E) or inhibitory (I) population is given by

$$V_i^{E/I}(t+1) = \left[\mu V_i^{E/I}(t) + I_e + \frac{J}{N} \sum_{j=1}^{N_E} X_j^E(t) - \frac{gJ}{N} \sum_{j=1}^{N_I} X_j^I(t) \right] \left(1 - X_i^{E/I}(t) \right), \quad (5)$$

where J is the synaptic coupling strength, g is the inhibition to excitation (E/I) coupling strength ratio, μ is the leak time constant, and I_e is an external current. The total number of neurons in the network is $N = N_E + N_I = 10^5$, where the fractions of excitatory and inhibitory neurons are kept fixed at $p = N_E/N = 0.8$ and $q = N_I/N = 0.2$, respectively, as reported for cortical data [31]. Note that the membrane potential is reset to zero in the time step following a spike.

At any time step, a neuron fires according to a piecewise linear sigmoidal probability $\Phi(V)$,

$$\Phi(V) \equiv P(X = 1|V) = \Gamma(V - \theta) \Theta(V - \theta) \Theta(V_S - V) + \Theta(V - V_S), \quad (6)$$

where $\theta = 1$ is the firing threshold, Γ is the firing gain constant, $V_S = 1/\Gamma + \theta$ is the saturation potential, and $\Theta(x > 0) = 1$ (zero otherwise) is the step function. For simplicity, the parameter $\mu = 0$ is chosen without lack of generality, since it does not change the phase transition of the model [30]. The external current $I_e > V_S$ is used only to spark a new avalanche in a single excitatory neuron when the network activity dies off (it is kept as $I_e = \theta$ otherwise).

This model is known to present a directed percolation critical point [30] at $g_c = p/q - 1/(q\Gamma J) = 1.5$ (for $\Gamma = 0.2$ and $J = 10$), such that $g < g_c$ is the active excitation-dominated (supercritical) phase and $g > g_c$ corresponds to the inhibition-dominated absorbing state (subcritical). The synapses in the critical point g_c are dynamically balanced: fluctuations in excitation are immediately followed by counter fluctuations in inhibition [30]. The initial condition of the simulations has all neurons quiescent except for a seed neuron to spark activity. This procedure was repeated whenever the system went back to the absorbing state.

B. Probabilistic cellular automaton model

The robustness of our findings was cross-checked using probabilistic cellular automata in a random network [32]. This model closely resembles a standard branching process and is known to mimic the changing inhibition-excitation levels of cortical cultures [33].

Each site i ($i = 1, \dots, N$) has 5 states: the silent state, $s_i = 0$, the active state, $s_i = 1$, corresponding to a spike, and the remaining three states, $s_i = 2, 3, 4$, in which the site will not respond to incoming stimuli (refractory states). Each site receives input from K presynaptic neighbors which are randomly selected at the start and kept fixed throughout the simulations. A quiescent site i becomes excited ($s_i(t) = 0 \rightarrow s_i(t+1) = 1$) with probability p_{ij} if a presynaptic neighbor j is active at time t . All presynaptic neighbors are swept and independently considered at each time step, so that

$$P(s_i(t+1) = 1 | s_i(t) = 0) = 1 - (1 - h_i) \prod_{j \in \mathcal{N}(i)}^K [1 - p_{ij}s_j(t)], \quad (7)$$

where h_i is the probability of unit i spiking due to an external stimulus and $\mathcal{N}(i)$ is the set of presynaptic neighbors of i . The remaining transitions happen with probability 1, including the transition $4 \rightarrow 0$ that returns the site to its initial quiescent state. The time step of the model corresponds to 1 ms.

We initially choose the random variables $\{p_{ij}\}$ from a uniform distribution in the interval $[0, 2\lambda/K]$. The so-called branching ratio $\lambda = K\langle p_{ij} \rangle$ is the control parameter of the model. This model undergoes a MF-DP phase transition at $\lambda = \lambda_c = 1$ [32]. For $\lambda < 1$, the system is in the subcritical phase and eventually reaches the absorbing state ($s_i = 0, \forall i$). For $\lambda > 1$, the system presents self-sustained activity, i.e. a nonzero stationary density of population firings (the supercritical phase).

In our simulations we used $K = 10$ neighbors for each of the $N = 10^5$ sites. Similarly to the spiking neuronal network model, a single random neuron was stimulated ($h_i = 1$) only when the system reached the absorbing state, sparking the network activity and subsequently being set back to $h_i = 0$. The initial condition was set with a single randomly chosen site active and the others in the silent state.

C. Experimental data acquisition

We used 5 rats Long-Evans (*Rattus norvegicus*) (male, 280-360 g, 2-4 months old). They were obtained from the animal house of the Laboratory of Computational and Systems Neuroscience, Department of Physics, Federal University of Pernambuco (UFPE).

The rats were maintained in the light/dark cycle of 12 h and their water and food were *ad libitum*.

The experimental protocol was approved by the Ethics Committee on Animal Use (CEUA) of UFPE (CEUA: 23076.030111/2013-95 and 12/2015), in accordance with the basic principles for research animals established by the National Council for the Control of Animal Experimentation (CONCEA).

The animals were anesthetized with urethane (1.55 g/kg), diluted at 20% in saline, in 3 intraperitoneal (i.p.) injections, 15 min apart. The rats were placed in a stereotaxic frame and the coordinates to access the primary visual cortex (V1) were marked (Bregma: AP = -7.2, ML = 3.5) [34]. A cranial window in the scalp was opened at this site with an area of approximately 3 mm^2 .

In order to record extra-cellular voltage, we used a 64-channels multielectrode silicon probe (Neuronexus technologies, Buzsaki64spL-A64). This probe has 60 electrodes disposed in 6 shanks separated by $200 \text{ }\mu\text{m}$, 10 electrodes per shank with impedance of 1–3 MOhm at 1 kHz. Each electrode has $160 \text{ }\mu\text{m}^2$ and they are in staggered positions $20 \text{ }\mu\text{m}$ apart.

The acquired data was sampled at 30 KHz, amplified and digitized in a single head-stage (Intan RHD2164) [35]. We recorded spontaneous activity, during long periods (≥ 3 hours). We used the open-source software Klusta to perform the automatic spike sorting on raw electrophysiological data [36]. The automatic part is divided in two major steps, spike detection and automatic clustering. The first step detects action potentials and the second one arrange those spikes into clusters according to their similarities (waveforms, PCA, refractory period). After the automatic part, all formed clusters are reanalyzed using the graphic interface phy kwikGUI¹. Manual spike sorting allows the identification of each cluster of neuronal activity as single-unit activity (SUA) or multi-unit activity (MUA). We use both SUA and MUA clusters for our study.

D. Avalanche analysis with CV parsing

To study neuronal avalanches at different levels of spiking variability, we segment both the neurophysiological and simulated data in non-overlapping windows of width $w = 10 \text{ s}$ (unless otherwise stated). Each of these 10 s epochs is subdivided in non-overlapping intervals $\{\zeta_j\}$ of duration $\Delta T = 50 \text{ ms}$ (unless otherwise stated) in which we estimate the population spike-count rate R_j . We then calculate the coefficient of variation (CV) for the i -th 10 s window:

$$CV_i = \frac{\sigma_i}{\mu_i}, \quad (8)$$

where CV is dimensionless, and σ_i and μ_i correspond to the standard deviation and the mean of $\{R_j\}$, respectively.

¹ <https://github.com/cortex-lab/phy>

For each 10 s window with a particular CV level, we proceed with the standard avalanche analysis of Beggs and Plenz [1]. The summed population activity is sliced in non-overlapping temporal bins of width $\Delta t = \langle ISI \rangle$ (the average inter-spike interval). Population spikes preceded and followed by silence define a spike avalanche. The number of spikes correspond to the avalanche size S , whereas the number of time bins spanned by the avalanche is its duration T . Following this methodology, we associate each 10 s CV_i window with its corresponding set of n_i avalanche sizes $\mathbf{S}_i \equiv \{S_{i1}, S_{i2}, \dots, S_{in_i}\}$ and durations $\mathbf{T}_i \equiv \{T_{i1}, T_{i2}, \dots, T_{in_i}\}$.

To estimate the avalanche exponents τ and τ_t , we first ranked the sets $\{\mathbf{S}_i\}$ and $\{\mathbf{T}_i\}$ according to their CV values. Next, in order to increase the number of samples while preserving the level of spiking variability, we pooled NB consecutive ranked blocks of similar CV values ($NB = 50$ unless otherwise stated). For each set of NB blocks we calculated the average coefficient of variation $\langle CV \rangle$. The exponents of the size and duration distributions were obtained via a Maximum Likelihood Estimator (MLE) procedure [37–39] on a discrete power-law distribution

$$f(x) = \frac{1}{\sum_{x=x_{min}}^{x_{max}} \left(\frac{1}{x}\right)^\alpha} \left(\frac{1}{x}\right)^\alpha. \quad (9)$$

The standard choice of fitting parameters, for both experimental and subsampled simulated data, was $S_{min} = 2$ and $S_{max} = 100$ for size distributions and $T_{min} = 2$ and $T_{max} = 30$ for duration distributions. The exceptions to this choice were for the data shown in Figure 4C and 4D, due to a change of orders of magnitude in the number of neurons sampled. The specific parameters for these cases are shown in Table I.

After the MLE fit we use the Akaike Information Criterion (AIC) as a measure of the relative quality of a

given statistical model for a data set:

$$AIC = 2k - 2\ln(\hat{L}) + \frac{2k^2 + 2k}{N - k - 1}, \quad (10)$$

where \hat{L} is the likelihood at its maximum, k is number of parameters and N the sample size [40]. Starting from the principle that lower AIC indicates a more parsimonious model, we define $\Delta \equiv AIC_{ln} - AIC_{pl}$, where AIC_{ln} and AIC_{pl} correspond to the AIC of a log-normal and a power-law model, respectively. Therefore, $\Delta > 0$ implies that a power-law model is a better fit to the data than a log-normal. Our scaling relation analyses were restricted to distributions that satisfied $\Delta > 0$.

E. Pairwise correlations

Pairwise spiking correlations were estimated using only the SUA or the simulated data in the following way: first, for each cell k we obtain a spike count time series $R^{(k)}(t)$ at millisecond resolution ($\Delta T = 1$ ms), then each spike count time series $R^{(k)}$ is convolved with a kernel $h_{t_1, t_2}(t)$ to estimate the k -th mean firing rate $n^{(k)}(t)$:

$$n^{(k)}(t) = h_{t_1, t_2}(t) * R^{(k)}(t), \quad (11)$$

where $h_{t_1, t_2}(t)$ is a Mexican-hat kernel obtained by the difference between zero-mean Gaussians with standard deviations $t_1 = 100$ ms and $t_2 = 400$ ms [41]. The $n_k(t)$ are used to calculate the spiking correlation coefficient between two units k and l :

$$r^{(k, l)} = \frac{\text{Cov}(n^{(k)}, n^{(l)})}{\sqrt{\text{Var}(n^{(k)}) \text{Var}(n^{(l)})}}, \quad (12)$$

where Var and Cov are the variance and covariance over t , respectively.

III. RESULTS

A. Avalanches in the fully sampled model

We start by illustrating the second order phase transition that the model undergoes at a critical value $g_c = 1.5$ of the inhibition parameter [30]. As shown in Figure 1A, the stationary density of active sites $\bar{\rho}$ is positive for $g < g_c$ (the supercritical regime) and null for $g > g_c$ (the subcritical regime).

At the critical point $g = g_c$, the distribution of avalanche sizes and duration obey the expected power laws (Equations (1) and (2)) with exponents $\tau = 3/2$ and $\tau_t = 2$ [30]. Subcritical avalanches are exponentially distributed, whereas the supercritical distribution has a trend to display large avalanches in space and time (Figure 1B and C). Both sides of the scaling law in Equation (4) independently agree, since the fit to $\langle S \rangle(T)$ yields

TABLE I. Limits chosen for the calculation of the α exponent (Equation 9) via Maximum Likelihood Estimator (MLE) only for the data shown in Figure 4C and D ($\Delta t = 1$ ms). See text for details.

n	Size distribution		Duration distribution	
	S_{min}	S_{max}	T_{min}	T_{max}
100	2	30	2	15
200	2	100	2	50
500	2	200	2	70
1000	2	200	2	70
2000	2	300	3	100
5000	2	500	4	100
10000	5	3000	5	150
20000	5	5000	5	200
30000	10	10000	10	200
40000	10	10000	10	250
50000	10	10000	10	300
100000	10	20000	10	300

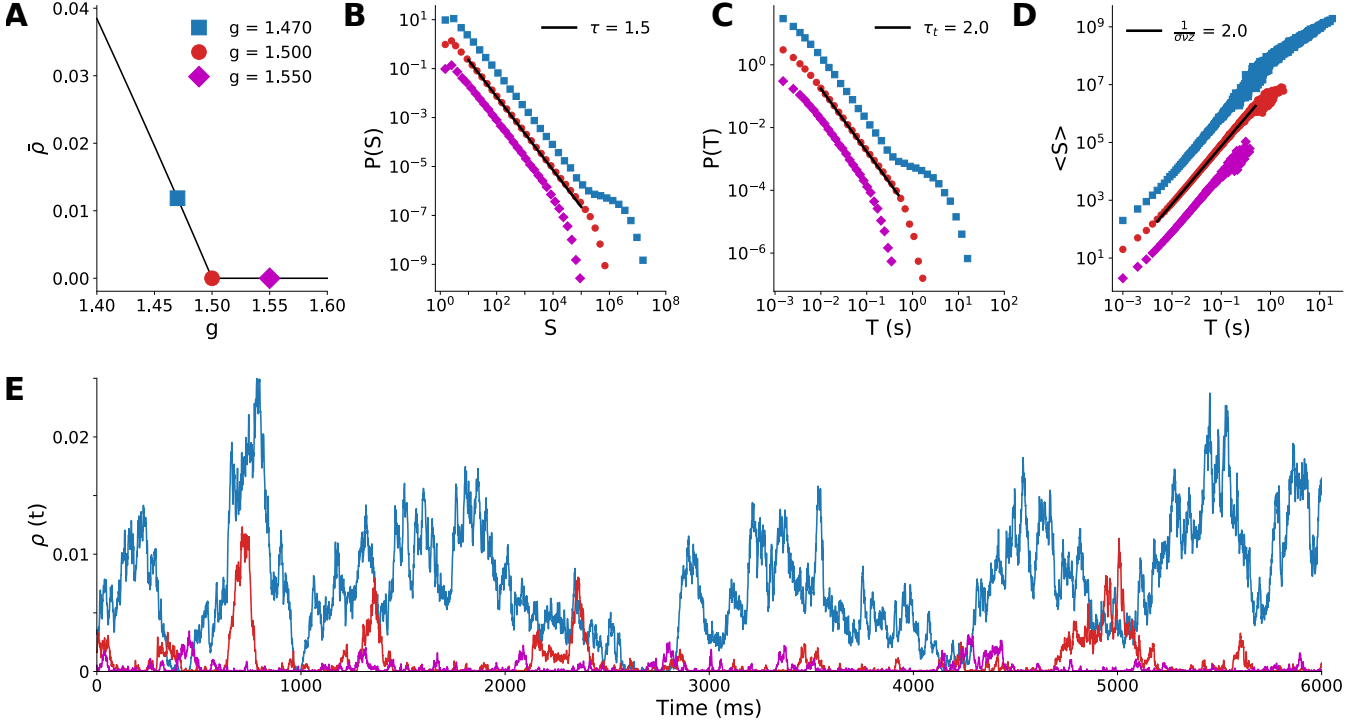


FIG. 1. Spiking model results with full sampling. Behavior of the spiking model ($N = 10^5$) for different values of the control parameter g . (A) Stationary density of firings $\bar{\rho}$ as a function of the inhibition strength g (critical point is the red circle at $g_c = 1.5$). Solid line is the mean-field solution [30], points are simulation results. Distribution of avalanche sizes (B) and duration (C) for the subcritical ($g > g_c$), critical ($g = g_c$) and supercritical ($g < g_c$) regimes. (D) Average avalanche size $\langle S \rangle$ of a given duration (T). (E) Time series of the density of active sites for the three regimes.

$1/(\sigma\nu z) = 2$ on the critical point (Figure 1D). Figure 1E shows typical time series of firing events for the three regimes. These exponents and dynamic behavior of the model is typical of a system undergoing a MF-DP phase transition.

B. Comparison of subsampled model and experiments stratified by CV

We now revisit the model by subjecting it to the same constraints that apply to experimental datasets [20] and compare the results between the two. More specifically: 1) data analysis necessarily uses only a tiny fraction of the total neurons in the system and 2) in urethane-anesthetized rats, cortical spiking variability is a proxy for cortical states [23] and changes a lot during the hours-long recordings [21, 22].

Starting with the experimental results, Figure 2A shows the time series of the coefficient of variation (CV) of the population spiking activity. The lowest CV values correspond to asynchronous spiking activity, whereas the highest values correspond to more synchronized activity (both shown in Figure 2B). When we parsed the data by CV percentiles and evaluated neuronal avalanches for different percentiles, the distributions varied accordingly,

with exponents τ , τ_t and $1/(\sigma\nu z)$ varying continuously across the CV range (Figure 2C) as expected [20].

Can the MF-DP spiking network model reproduce these experimental results? We found that by sampling only a few neurons out of the entire network, indeed it can. We sample only $n = 100$ neurons out of $N = 10^5$, a number that is of the same order as the amount of neurons captured in our empirical data [20]. Then, we apply to the subsampled simulation data exactly the same pipeline used for experiments (Section IID).

In the model, we change the E/I level g to control for the variability level CV . For a fixed value of parameter g , CV is a bell-shaped distribution with finite variance. The $CV(t)$ time series of the model for a single g does not present the dynamical complexity observed experimentally (compare Figures 2A and 2D). By varying g within a narrow interval around the critical point g_c , the CV distribution of the model covers the values observed experimentally (Figure 2D), with less synchronous behavior for low CV and more synchronous activity for high CV (Figure 2E; the full behavior of the CV distribution as a function of parameter g is shown in Figure A1A). Parsing the data by CV and running the avalanche statistics for the subsampled model, we obtain scaling exponents that vary continuously in remarkable similarity to what is observed in the experimental data (Figure 2F).

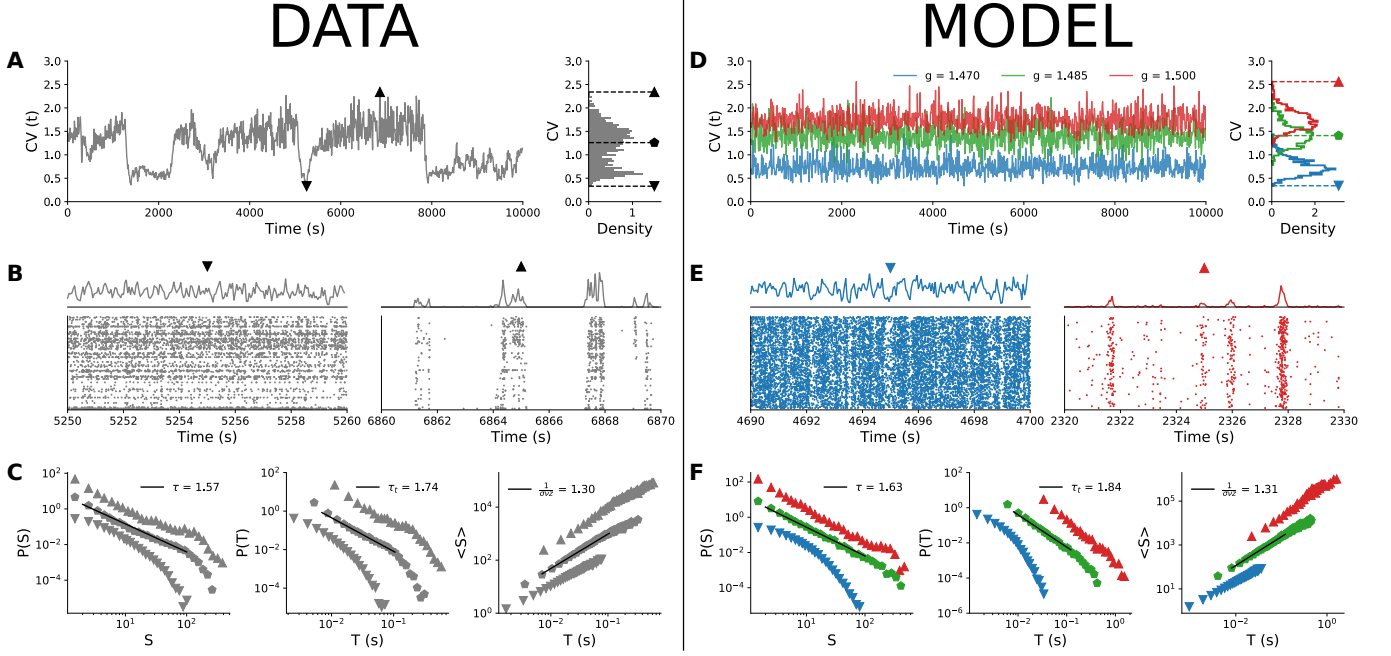


FIG. 2. Comparison between empirical data and subsampled spiking model. CV time series and distribution for **(A)** experimental data (single animal) and **(D)** model with $n = 100$. Raster plots and population firing rate in cases of low (∇) and high (Δ) values of CV for **(B)** experimental data and **(E)** model. Scaling exponents τ , τ_t and $1/(\sigma\nu z)$ for three different values of CV (denoted by different symbols): **(C)** experimental data and **(F)** model. For both experimental data and model, $w = 10$ s.

To ensure criticality, we must require that the scaling relation in Equation (4) is satisfied. Figure 3A shows the independent experimental fits for the left- and right-hand sides of Equation (4). The crossing at $CV_* \simeq 1.46 \pm 0.08$ is consistent with a phase transition at an intermediate point between asynchronous and synchronous behavior [20]. In the crossing CV_* , we obtain $\tau_* = 1.54 \pm 0.12$, $\tau_{t*} = 1.73 \pm 0.18$ and $1/(\sigma\nu z)_* = 1.30 \pm 0.02$. Plotting τ versus τ_t , the experimental data scatter along the line with slope given by $1/(\sigma\nu z)_*$ for different values of CV (Figure 3B). These results are in agreement with those of Fontenele et al. [20], again suggesting an incompatibility with the MF-DP universality class.

The results for the subsampled spiking model, however, suggest otherwise. We do exactly the same procedure with the subsampled model and find a similar CV for the crossing of the critical exponents, $CV_{*model} \simeq 1.41 \pm 0.05$, when controlling for the E/I ratio g very close to the critical point $g_c = 1.5$ (Figure 3C). On the crossing CV_{*model} , we obtain $\tau_* = 1.65 \pm 0.02$, $\tau_{t*} = 1.87 \pm 0.03$ and $1/(\sigma\nu z)_* = 1.34 \pm 0.02$. Note that these critical exponents are not the real exponents of the model. In fact, they are apparent exponents generated by subsampling the network activity. The real critical exponents are $\tau = 3/2$, $\tau_t = 2$ and $1/(\sigma\nu z) = 2$ (as we showed in Figure 2).

To reproduce the experimental results, the control interval of g was slightly biased towards the supercritical range: $g_{min} \simeq 1.47 \leq g \leq g_{max} \simeq 1.50$. Our model pre-

dicts, then, that the whole range of experimental results is produced by fluctuations of only about 2% around the critical point (Figure 3D). For instance, for $g = 1.55$ (3% above the critical point in the subcritical regime), the scaling relation is no longer satisfied and the measured exponents fall far away from the linear relation observed experimentally in the (τ, τ_t) plane (Figure 3D).

This result shows that the MF-DP phase transition under subsampling conditions is capable of reproducing a whole range of experimentally observed avalanches due to different CV . To test the robustness of our findings, we employ exactly the same procedure to a simpler model, the probabilistic cellular automaton (Section II B). This model is also knowingly of the MF-DP type [32], but has a random network topology. All the results were similar (see Figure B1), showing that the apparent exponents are a direct consequence of subsampling.

C. Dependence on sampling fraction and time bin width

How robust are the results of the model against variation in the sampling size (n) and time bin width (Δt)? First, we consider the time bin width as the population interspike interval $\Delta t = \langle ISI \rangle$. The minimum sampling size we employ is $n = 30$ so that power laws still satisfy Akaike's Information Criterion. The agreement of both sides of the scaling law enhances with growing sampling

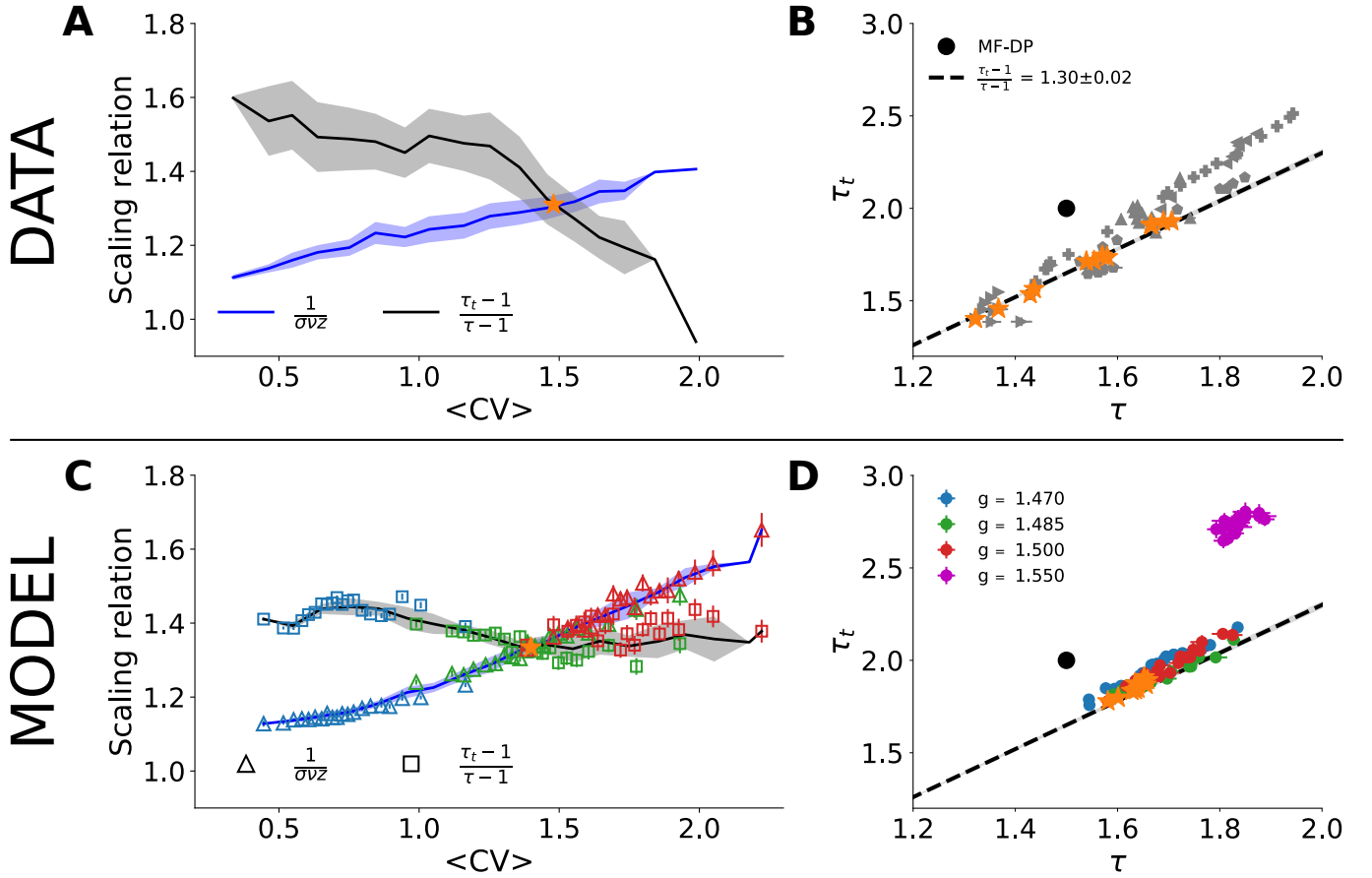


FIG. 3. Scaling relation and parametric plot of avalanche exponents. Right- and left-sides of Equation (4) (line and shade are average and standard deviation across the group) as a function of the average CV for (A) experimental data and (C) subsampled model ($n = 100$; note that color code and values of g are the same as in Figures 2D and 2F). Scatter plot in the (τ, τ_t) plane for (B) experimental data and (D) subsampled model. In both cases, $\Delta t = \langle ISI \rangle$ and $w = 10$ s. The star points in (B) and (D) indicate the values of τ and τ_t that satisfied Equation (4) in (A) and (C).

fraction (Figure 4A and B). However, $\langle ISI \rangle$ decreases with the number of neurons sampled (inset of Figure 4B). When the natural bin decreases below 1 ms (the time step of the model), the analysis no longer makes sense. As n increases, the relation between τ and τ_t converges to the apparent critical scaling that fits experimental results (Figure 4B).

To check whether we recover the MF-DP real exponents from their apparent values as n increases, we choose the smallest time bin possible, $\Delta t = 1$ ms. We observe that for a small fraction of sampled units ($n/N \sim \mathcal{O}(10^{-2})$) the scaling relation (Equation 4) is satisfied (Figure 4C) with the apparent critical exponents that match the experimental results (Figure 4D). In fact, the scaling relation in Equation 4 is satisfied for a range of CV values (inset of Figure 4C). Increasing the sampling further ($n/N \sim \mathcal{O}(10^{-1})$), the scaling relation ceases to be satisfied (Figure 4C) and the avalanche exponents get separated from the experimental scaling relation (Figure 4D). But as $n \rightarrow N$, the MF-DP scaling relation is recovered (as it should).

We have further tested the robustness of these find-

ings by varying the time bin width used to defined avalanches ($0.75 \leq \Delta t / \langle ISI \rangle \leq 2$). We observed that experiments and model have very similar behavior (Figures C1A and C1B). Furthermore, both model and experiments are virtually insensitive to the width of the CV window w (Figures C1C and C1D).

D. Pairwise correlation structure

We also tested the correlation structure of the model and compared it to experimental results. In the literature on cortical states, asynchronous states are associated with pairwise spiking correlations $r^{(k,l)}$ which are distributed around an average \bar{r} close to zero, whereas synchronous states have positive average [23]. This is quantified in Figure 5A, where \bar{r} is shown to increase monotonically with CV . For the experimental data, \bar{r} reaches zero within the standard deviation of the distribution for sufficiently small CV .

Compared with the experimental results, the spiking

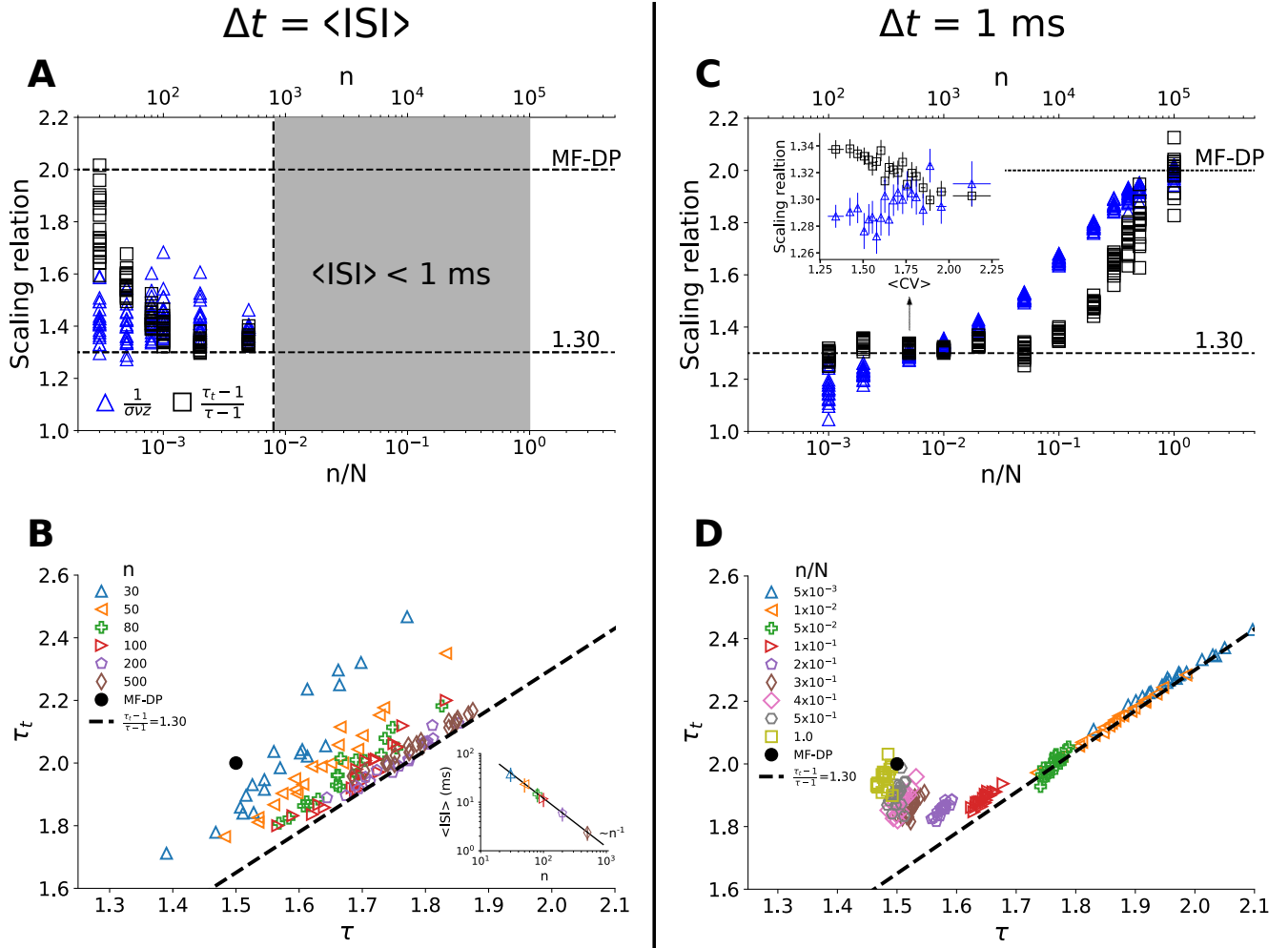


FIG. 4. Dependence of the apparent critical exponents on the sampling parameters. In (A) and (C), we show both sides of the scaling relation (Equation 4) for *all* values of CV observed in the simulations. For each value of n/N , one has the equivalent of the projection of Figure 3C onto its vertical axis. For $\Delta t = \langle ISI \rangle$, (A) the scaling relation is satisfied for increasing number of sampled neurons (B) with exponents that agree with experimental data. Since $\langle ISI \rangle$ decreases with n (inset of (B)), this analysis breaks down when n is so large that $\langle ISI \rangle$ becomes smaller than 1 ms (grey region in (A)), which is the time step of the simulations. For $\Delta t = 1 \text{ ms}$, (C) the scaling relation is satisfied for small n/N , within a relatively wide range of CV values (inset of (C)). For $n/N \rightarrow 1$, results converge to MF-DP values ((C) and (D)), as expected. Simulations with $N = 10^5$ and $g = 1.5$.

model with inhibition generally overestimates \bar{r} (Figure 5A). This could be due to its all-to-all connectivity. The cellular automaton model on a random graph yields quantitatively better results (Figure 5B). In either case, we observe again that, just like for the scaling relation (Figure 3), the correlation structure of the experimental data is relatively well reproduced by very small deviations around critical parameter values.

IV. DISCUSSION AND CONCLUSIONS

We revisited the results recently published by Fontenele et al. [20] by repeating their analyses on new experimental data and two different models. To test the

idea that the urethanized cortex hovers around a critical point, we stratified the avalanche analyses across cortical states. For the new experimental data, we verified that the scaling relation combining the three exponents (Equation 4) is indeed satisfied at an intermediate value CV_* , away from the synchronous and asynchronous extremes. At this critical value, the three exponents differ from those of the MF-DP universality class, thus confirming previous findings [20].

We addressed whether the exponents of the MF-DP universality class and those observed experimentally could be reconciled, despite their disagreement. In other words, we return to the question: if the brain is critical, what is the phase transition? Do the experimental results presented here and in Fontenele et al. [20] refute

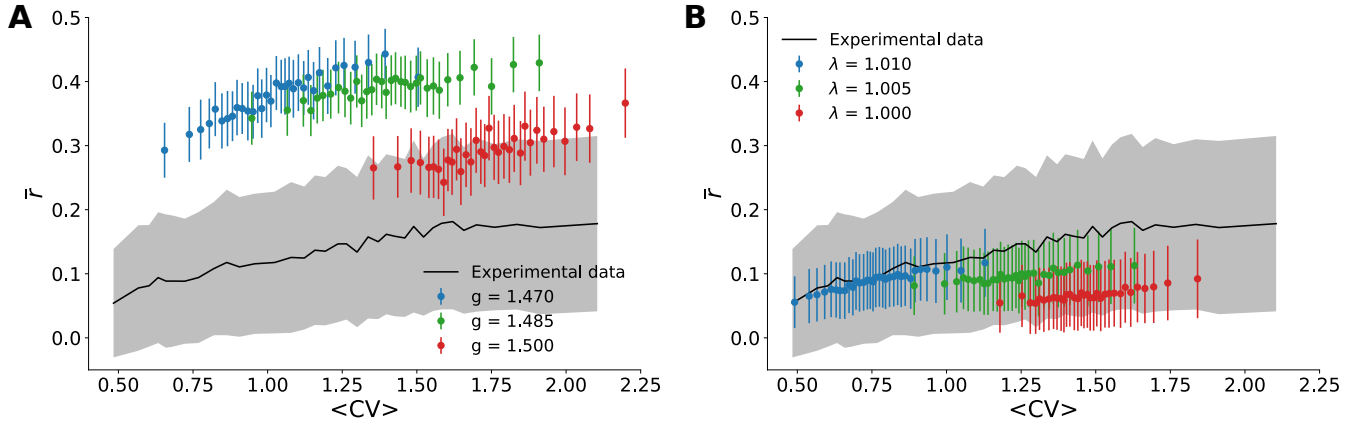


FIG. 5. Correlation structure. The experimental pairwise correlation of firing rates is shown as a function of $\langle CV \rangle$ (black line is the average \bar{r} , while gray shading is the standard deviation of the distribution). It is compared with theoretical results for (A) the spiking neuronal network with $n = 100$ sampled neurons, and (B) the cellular automaton model with $n = 500$ sampled sites.

branching-process-like models as explanations?

To answer these questions, we relied on two models: an E/I spiking neuronal network in an all-to-all graph; and a probabilistic excitable cellular automaton in a random graph. Despite the simplicity and limitations of these models (which we discuss below), they have a fundamental strength that led us to choose them: they are very well understood analytically. In both cases, mean-field calculations agree extremely well with simulations, so that we are safe in locating the critical points of these models [30, 32]. This is very important for our purposes, because it allows us to test whether the models can reproduce the data and, if so, how close to the critical point they have to be. Besides, their universality class is also well determined: the exponents shown in Figures 1B, 1C and 1D are those of with MF-DP.

The crucial point is that the results in Figure 1 are based on avalanches which are measured by taking into account *all* simulated units of the model, a methodological privilege that is not available to an experimentalist measuring spiking activity of a real brain with current technologies. In fact, a considerable amount of work has shown that subsampling can have a drastic effect on the avalanche statistics of models [12, 24–29]. Therefore, here we set out to test whether MF-DP models could yield results nominally incompatible with that universality class if they were analyzed under the same conditions as the data, i.e. with CV parsing and severe subsampling.

Both subsampled models can quantitatively and qualitatively reproduce the central features of the experimental results. The scaling relation (Equation 4) is satisfied at an intermediate value $\langle CV \rangle_*$, with the correct qualitative behavior of both sides of the equation: $1/(\sigma\nu z)$ increases with CV , while $(\tau_t - 1)/(\tau - 1)$ decreases (see Figures 3A, 3C and B1D). In fact, the values of $\langle CV \rangle_*$, and those of the apparent exponents of the MF-DP models, τ_* , τ_{t*} , and $1/(\sigma\nu z)_*$, agree with the experiments

within errorbars. Moreover, even away from the point $\langle CV \rangle_*$ where Equation (4) is satisfied, the spread of the exponents τ and τ_t of the subsampled models follows an almost linear relation (Figures 3D and B1E), in good agreement with not only our experimental results (Figure 3B), but also with those of other experimental setups [20]. When we sample from the whole network, we recover the true critical exponents of the model, confirming that spatial subsampling and temporal binning are sufficient ingredients to push the urethanized rats' brains critical exponents toward apparent values, hiding its putative true critical phase transition.

Knowing analytically the critical points of the models, we can check in which parameter range they successfully reproduce the experimental results. As it turns out, the scaling relation and the linear of spread of exponents are reproduced by the subsampled models only if they are tuned within a narrow interval around their critical points. The model still fits well the urethanized cortex data up to 3% away towards the supercritical state. This corroborates the hypothesis that the brain operates in a quasicritical state [42] that is slightly supercritical [30, 43]. This contrasts with claims that the brain might operate slightly subcritically [27]. Note that if the model becomes too subcritical, the size and duration exponents fall very far apart from the experimentally observed linear relation (Figure 3D). If it is too supercritical, there are not enough silent windows to distinguish avalanches in the first place. This discrepancy is a topic for further investigation, since our models have operated in the limit of zero external field (i.e., external stimuli was only employed to generate an avalanche). Priesemann et al. [27], for instance, tried to follow a balance between internal coupling and external stimulus in order to maintain an average firing rate. Whether that different approach would lead to significant changes to our results remains to be investigated.

Despite the small variation of the model E/I levels controlled by g , the variation of CV is large enough to essentially cover the range of experimentally observed values (Figures 2A, 2D and B1B). This is due in part to the fact that we evaluated CV within finite windows of width $w = 10$ s. In Figure D1, we show that the standard deviation of CV is a decreasing function of the time used to estimate it. This implicates that a better resolution for experimental CV can be obtained by increasing this time windows to 20 s. It is important to note, however, that in experiments one needs to reach a good trade-off between a better statistical definition of CV and not mixing different cortical states due to the nonstationarity characteristic of the urethane preparation (as depicted in Figure 2A).

Perhaps even more important than the range of CV values obtained around the critical point of the models is the richness of the experimentally observed temporal evolution of CV (Figure 2A). The model needs to be fine tuned to different values of E/I levels in order to get different average values of CV . This is one of the limitations of the models which would be worth addressing next. One possibility would be to replace static models (i.e., with fixed control parameters) with ones with plasticity, in which coupling parameters are themselves dynamic variables and the critical point is obtained via quasicritical self-organization [30, 43–47].

Another limitation of the models is their simple topology, which in future works could be improved to come closer to cortical circuitry [48]. This would likely come at the cost of foregoing analytical results to start with, thus augmenting the computational efforts involved. But it would certainly allow to probe the robustness of the results presented here against more realistic topologies. On the other hand, there is quantitative agreement between the apparent exponents of both models (each having a different topology) with the experimental exponents. This suggests that at the scale of the present phenomenology, the average topology should play a minor role.

The fact that subsampling seems to be a crucial ingredient for explaining the data is a double-edged sword. On the one hand, it allowed us here to reconcile MF-DP

models with results for spiking data in the anesthetized rat cortex. On the other hand, note that even measurements which should in principle be less prone to subsampling, such as LFP results in the visual cortex of the turtle [11], still fall on the same scaling line of τ versus τ_t (Figure 3B) as those of spiking data [20], both having apparent non-MF-DP critical exponents. This issue is not addressed by the current model and deserves further investigation. Our results point only to MF-DP models as sufficient, not as necessary, to explain the observed phenomenology. So it is at least conceivable that different models with different phase transitions [49–51] could also yield non-trivial true or apparent exponents compatible with the data, even without subsampling [20].

Finally, our simulation results underscore the methodological vulnerabilities of assessing criticality exclusively via avalanche analysis. Not only are MLE power-law fits sensitive to parameters but even a more stringent scaling analysis can lead to non-trivial apparent exponents which are an artifact of subsampling, as we have shown. Therefore, the development of additional figures of merit, such as control and order parameters, susceptibilities and others [19, 52–58], remains a very important line of research to strengthen studies of brain criticality.

V. ACKNOWLEDGMENT

The authors acknowledge Fundao de Amparo à Ciencia e Tecnologia de Pernambuco (FACEPE) (grants APQ-0642-1.05/18 and APQ-0826-1.05/15), Universidade Federal de Pernambuco, Conselho Nacional de Desenvolvimento Científico e Tecnológico (CNPq, grants 425329/2018-6 and 301744/2018-1), Coordenação de Aperfeiçoamento de Pessoal de Nível Superior (CAPES) and FAPESP (grant 2018/09150-9). This paper was produced as part of the activities of Research, Innovation and Dissemination Center for Neuromathematics (grant No. 2013/07699-0, S. Paulo Research Foundation – FAPESP). We thank Osame Kinouchi for discussions and a critical read of this manuscript.

-
- [1] J. M. Beggs and D. Plenz, “Neuronal avalanches in neocortical circuits,” *J. Neurosci.*, vol. 23, pp. 11167–11177, 2003.
 - [2] J. M. Beggs, “The criticality hypothesis: how local cortical networks might optimize information processing,” *Philos. Trans. R. Soc. A*, vol. 366, pp. 329–343, 2007.
 - [3] D. R. Chialvo, “Emergent complex neural dynamics,” *Nat. Phys.*, vol. 6, pp. 744–750, 2010.
 - [4] W. L. Shew and D. Plenz, “The functional benefits of criticality in the cortex,” *Neuroscientist*, vol. 19, pp. 88–100, 2013.
 - [5] T. E. Harris, *The Theory of Branching Processes*. Springer, 1963.
 - [6] M. A. Muñoz, R. Dickman, A. Vespignani, and S. Zapperi, “Avalanche and spreading exponents in systems with absorbing states,” *Phys. Rev. E*, vol. 59, pp. 6175–6179, 1999.
 - [7] J. J. Binney, N. J. Dowrick, A. J. Fisher, and M. E. J. Newman, *The Theory of Critical Phenomena: An Introduction to The Renormalization Group*. Oxford: Oxford University Press, 1992.
 - [8] H. K. Janssen, “On the nonequilibrium phase transition in reaction-diffusion systems with an absorbing station-

- ary state,” *Z. Physik B - Condensed Matter*, vol. 42, pp. 151–154, 1981.
- [9] P. Grassberger, “On phase transitions in schlg’s second model,” *Z. Physik B - Condensed Matter*, vol. 47, pp. 365–374, 1982.
- [10] J. Marro and R. Dickman, *Nonequilibrium Phase Transition in Lattice Models*. Cambridge: Cambridge University Press, 1999.
- [11] W. L. Shew, W. P. Clawson, J. Pobst, Y. Karimippanah, N. C. Wright, and R. Wessel, “Adaptation to sensory input tunes visual cortex to criticality,” *Nat. Phys.*, vol. 11, pp. 659–663, 2015.
- [12] T. L. Ribeiro, M. Copelli, F. Caixeta, H. Belchior, D. R. Chialvo, M. A. L. Nicolelis, and S. Ribeiro, “Spike avalanches exhibit universal dynamics across the sleep-wake cycle,” *PLoS One*, vol. 5, p. e14129, 2010.
- [13] J. M. Palva, A. Zhigalov, J. Hirvonen, O. Korhonen, K. Linkenkaer-Hansen, and S. Palva, “Neuronal long-range temporal correlations and avalanche dynamics are correlated with behavioral scaling laws,” *Proc. Natl. Acad. Sci. USA*, vol. 110, pp. 3585–3590, 2013.
- [14] A. Zhigalov, G. Arnulfo, L. Nobili, S. Palva, and J. M. Palva, “Relationship of fast- and slow-timescale neuronal dynamics in human MEG and SEEG,” *J. Neurosci.*, vol. 35, pp. 5385–5396, 2015.
- [15] J. Touboul and A. Destexhe, “Power-law statistics and universal scaling in the absence of criticality,” *Phys. Rev. E*, vol. 95, p. 012413, 2017.
- [16] J. P. Sethna, K. A. Dahmen, and C. R. Myers, “Crackling noise,” *Nature*, vol. 410, pp. 242–250, 2001.
- [17] N. Friedman, S. Ito, B. A. W. Brinkman, M. Shimono, R. E. L. DeVille, K. A. Dahmen, J. M. Beggs, and T. C. Butler, “Universal critical dynamics in high resolution neuronal avalanche data,” *Phys. Rev. Lett.*, vol. 108, p. 208102, 2012.
- [18] Z. Ma, G. G. Turrigiano, R. Wessel, and K. B. Hengen, “Cortical circuit dynamics are homeostatically tuned to criticality in vivo,” *Neuron*, vol. 104, pp. 655–664, 2019.
- [19] M. Girardi-Schappo and M. H. R. Tragtenberg, “Measuring neuronal avalanches in disordered systems with absorbing states,” *Phys. Rev. E*, vol. 97, p. 042415, 2018.
- [20] A. J. Fontenele, N. A. P. de Vasconcelos, T. Feliciano, L. A. A. Aguiar, C. Soares-Cunha, B. Coimbra, L. Dalla Porta, S. Ribeiro, A. J. Rodrigues, N. Sousa, P. V. Carelli, and M. Copelli, “Criticality between cortical states,” *Phys. Rev. Lett.*, vol. 122, p. 208101, 2019.
- [21] E. A. Clement, A. Richard, M. Thwaites, J. Ailon, S. Peters, and C. T. Dickson, “Cyclic and sleep-like spontaneous alternations of brain state under urethane anaesthesia,” *PLoS One*, vol. 3, p. e2004, 2008.
- [22] N. A. P. de Vasconcelos, C. Soares-Cunha, A. J. Rodrigues, S. Ribeiro, and N. Sousa, “Coupled variability in primary sensory areas and the hippocampus during spontaneous activity,” *Sci. Rep.*, vol. 7, p. 46077, 2017.
- [23] K. D. Harris and A. Thiele, “Cortical state and attention,” *Nat. Rev. Neurosci.*, vol. 12, p. 509, 2011.
- [24] V. Priesemann, M. H. J. Munk, and M. Wibral, “Subsampling effects in neuronal avalanche distributions recorded in vivo,” *BMC Neurosci.*, vol. 10, p. 40, 2009.
- [25] M. Girardi-Schappo, O. Kinouchi, and M. H. R. Tragtenberg, “Critical avalanches and subsampling in map-based neural networks coupled with noisy synapses,” *Phys. Rev. E*, vol. 88, p. 024701, 2013.
- [26] T. L. Ribeiro, S. Ribeiro, H. Belchior, F. Caixeta, and M. Copelli, “Undersampled critical branching processes on small-world and random networks fail to reproduce the statistics of spike avalanches,” *PLoS One*, vol. 9, p. e94992, 2014.
- [27] V. Priesemann, M. Wibral, M. Valderrama, R. Prpper, M. Le Van Quyen, T. Geisel, J. Triesch, D. Nikoli, and M. H. J. Munk, “Spike avalanches in vivo suggest a driven, slightly subcritical brain state,” *Front. Syst. Neurosci.*, vol. 8, p. 108, 2014.
- [28] A. Levina and V. Priesemann, “Subsampling scaling,” *Nat. Commun.*, vol. 8, p. 15140, 2017.
- [29] J. Wilting and V. Priesemann, “Between perfectly critical and fully irregular: A reverberating model captures and predicts cortical spike propagation,” *Cereb. Cortex*, vol. 29, pp. 2759–2770, 2019.
- [30] M. Girardi-Schappo, L. Brochini, A. A. Costa, T. T. A. Carvalho, and O. Kinouchi, “Synaptic balance due to homeostatically self-organized quasicritical dynamics,” *Phys. Rev. Research*, vol. 2, p. 012042(R), 2020.
- [31] P. Somogyi, G. Tamás, R. Lujan, and E. H. Buhl, “Salient features of synaptic organisation in the cerebral cortex,” *Brain Res. Rev.*, vol. 26, pp. 113–135, 1998.
- [32] O. Kinouchi and M. Copelli, “Optimal dynamical range of excitable networks at criticality,” *Nat. Phys.*, vol. 2, p. 348, 2006.
- [33] W. L. Shew, H. Yang, T. Petermann, R. Roy, and D. Plenz, “Neuronal avalanches imply maximum dynamic range in cortical networks at criticality,” *J. Neurosci.*, vol. 29, no. 49, pp. 15595–15600, 2009.
- [34] G. Paxinos and C. Watson, *The Rat Brain in Stereotaxic Coordinates: Hard Cover Edition*. Elsevier Science, 2007.
- [35] J. H. Siegle, A. C. Lpez, Y. A. Patel, K. Abramov, S. Ohayon, and J. Voigts, “Open Ephys: an open-source, plugin-based platform for multichannel electrophysiology,” *J Neural Eng.*, vol. 14, p. 045003, 2017.
- [36] C. Rossant, S. N. Kadir, D. F. M. Goodman, J. Schulman, M. L. D. Hunter, A. B. Saleem, A. Grosmark, M. Belluscio, G. H. Denfield, A. S. Ecker, *et al.*, “Spike sorting for large, dense electrode arrays,” *Nat. Neurosci.*, vol. 19, p. 634, 2016.
- [37] S. Yu, A. Klaus, H. Yang, and D. Plenz, “Scale-invariant neuronal avalanche dynamics and the cut-off in size distributions,” *PLoS One*, vol. 9, p. e99761, 2014.
- [38] A. Deluca and Á. Corral, “Fitting and goodness-of-fit test of non-truncated and truncated power-law distributions,” *Acta Geophys.*, vol. 61, pp. 1351–1394, 2013.
- [39] N. Marshall, N. M. Timme, N. Bennett, M. Ripp, E. Lautzenhiser, and J. M. Beggs, “Analysis of power laws, shape collapses, and neural complexity: new techniques and MATLAB support via the NCC toolbox,” *Front. Physiol.*, vol. 7, p. 250, 2016.
- [40] H. Akaike, “A new look at the statistical model identification,” *IEEE Trans. Automat. Contr.*, vol. 19, pp. 716–723, 1975.
- [41] A. Renart, J. de la Rocha, P. Bartho, L. Hollender, N. Parga, A. Reyes, and K. D. Harris, “The asynchronous state in cortical circuits,” *Science*, vol. 327, pp. 587–590, 2010.
- [42] J. A. Bonachela, S. de Franciscis, J. J. Torres, and M. A. Muñoz, “Self-organization without conservation: are neuronal avalanches generically critical?,” *J. Stat. Mech.*, p. P02015, 2010.

- [43] A. A. Costa, L. Brochini, and O. Kinouchi, “Self-organized supercriticality and oscillations in networks of stochastic spiking neurons,” *Entropy*, vol. 19, p. 399, 2017.
- [44] A. A. Costa, M. Copelli, and O. Kinouchi, “Can dynamical synapses produce true self-organized criticality?,” *J. Stat. Mech. Theory Exp.*, vol. 2015, p. P06004, 2015.
- [45] L. Brochini, A. A. Costa, M. Abadi, A. C. Roque, J. Stolfi, and O. Kinouchi, “Phase transitions and self-organized criticality in networks of stochastic spiking neurons,” *Sci. Rep.*, vol. 6, p. 35831, 2016.
- [46] J. G. F. Campos, A. A. Costa, M. Copelli, and O. Kinouchi, “Correlations induced by depressing synapses in critically self-organized networks with quenched dynamics,” *Phys. Rev. E*, vol. 95, p. 042303, 2017.
- [47] O. Kinouchi, L. Brochini, A. A. Costa, J. G. F. Campos, and M. Copelli, “Stochastic oscillations and dragon king avalanches in self-organized quasi-critical systems,” *Sci. Rep.*, vol. 9, p. 3874, 2019.
- [48] T. C. Potjans and M. Diesmann, “The cell-type specific cortical microcircuit: relating structure and activity in a full-scale spiking network model,” *Cereb. Cortex*, vol. 24, pp. 785–806, 2014.
- [49] S. di Santo, P. Villegas, R. Burioni, and M. A. Muñoz, “Landau–Ginzburg theory of cortex dynamics: Scale-free avalanches emerge at the edge of synchronization,” *Proc. Natl. Acad. Sci. U.S.A.*, vol. 115, no. 7, pp. E1356–E1365, 2018.
- [50] L. Dalla Porta and M. Copelli, “Modeling neuronal avalanches and long-range temporal correlations at the emergence of collective oscillations: Continuously varying exponents mimic M/EEG results,” *PLoS Comput. Biol.*, vol. 15, p. e1006924, 2019.
- [51] I. L. D. Pinto and M. Copelli, “Oscillations and collective excitability in a model of stochastic neurons under excitatory and inhibitory coupling,” *Phys. Rev. E*, vol. 100, p. 062416, 2019.
- [52] H. Yang, W. L. Shew, R. Roy, and D. Plenz, “Maximal variability of phase synchrony in cortical networks with neuronal avalanches,” *J. Neurosci.*, vol. 32, pp. 1061–1072, 2012.
- [53] E. Tagliazucchi, P. Balenzuela, D. Fraiman, and D. R. Chialvo, “Criticality in large-scale brain fMRI dynamics unveiled by a novel point process analysis,” *Front. Physiol.*, vol. 3, p. 15, 2012.
- [54] S. Yu, H. Yang, O. Shriki, and D. Plenz, “Universal organization of resting brain activity at the thermodynamic critical point,” *Front. Syst. Neurosci.*, vol. 7, p. 42, 2013.
- [55] G. Tkaik, T. Mora, O. Marre, D. Amodei, S. E. Palmer, M. J. Berry, and W. Bialek, “Thermodynamics and signatures of criticality in a network of neurons,” *Proc. Natl. Acad. Sci. U.S.A.*, vol. 112, pp. 11508–11513, 2015.
- [56] T. Mora, S. Deny, and O. Marre, “Dynamical criticality in the collective activity of a population of retinal neurons,” *Phys. Rev. Lett.*, vol. 114, p. 078105, 2015.
- [57] M. Girardi-Schappo, G. S. Bortolotto, J. J. Gonsalves, L. T. Pinto, and M. H. R. Tragtenberg, “Griffiths phase and long-range correlations in a biologically motivated visual cortex model,” *Sci. Rep.*, vol. 6, p. 29561, 2016.
- [58] N. Lotfi, A. J. Fontenele, T. Feliciano, L. A. Aguiar, N. A. de Vasconcelos, C. Soares-Cunha, B. Coimbra, A. J. Rodrigues, N. Sousa, M. Copelli, and P. V. Carelli, “Signatures of brain criticality unveiled by maximum entropy analysis across cortical states,” *arXiv e-prints*, 2020.

Appendix A: CV distribution as a function of model parameters

Here we illustrate the distribution of CV values as parameter values of the models are varied. In both cases, CV was estimated like in experimental data, i.e. for a subsampled number of units and during a finite window of time. Note that, as the net excitation decreases along the horizontal axes in Figure A1, the average values of CV initially increase, then saturate.

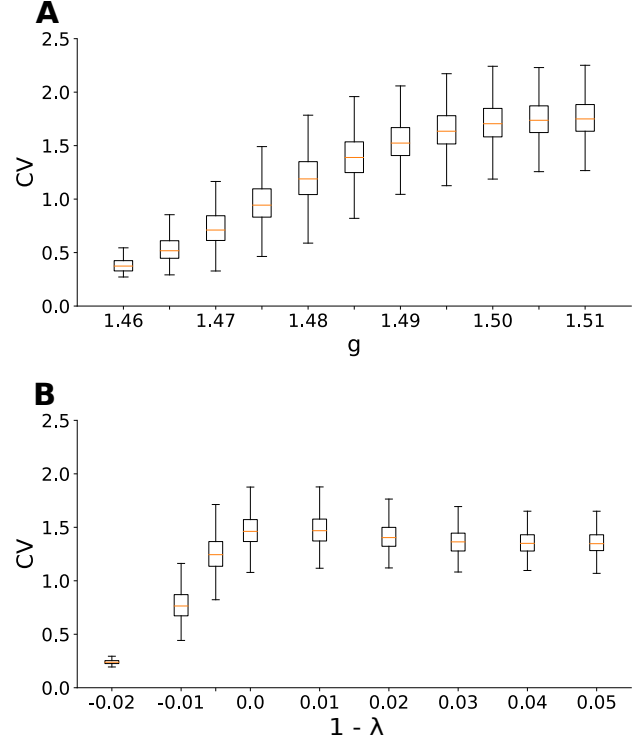


FIG. A1. CV distribution versus model parameters. Boxplots of CV as a function of parameter (A) g for the spiking model with excitation and inhibition and (B) $1 - \lambda$ for the probabilistic cellular automaton model. In both cases, $w = 10$ s, just like for experimental data. (A) $n = 100$. (B) $n = 500$.

Appendix B: Results for the cellular automaton model

Simulations for the cellular automaton model described in Section IIB of the main paper yielded results similar to those obtained for the spiking model. Figure B1 shows the same plots as in Figures 2 and 3, with similar values of the exponents and of the spiking variability at which the scaling relation in Equation (4) is satisfied: at $CV_*^{CA-model} = 1.30 \pm 0.05$, $\tau_*^{CA-model} = 1.71 \pm 0.03$, $\tau_{t*}^{CA-model} = 1.94 \pm 0.03$ and $1/(\sigma\nu z)_*^{CA-model} = 1.33 \pm 0.02$.

Note also the same tendency of the model to reproduce the data for slightly supercritical values with the coupling parameter ranging from $1.00 \leq \lambda \leq 1.01$. Fluctuations around the critical point $\lambda_c = 1$ in parameter space are therefore in the range of 1%.

Appendix C: Robustness with respect to time bin

In Figure 4 of the main text, we explore how the exponents τ and τ_t depend on the number of sampled units n and the choice of two different bins for the analysis of avalanches: $\Delta t = \langle ISI \rangle$ and $\Delta t = 1$ ms. Here, we probe further the robustness of the results for experimental and subsampled model data in the evaluation of $\langle CV \rangle_*$, τ_* , and τ_{t*} that satisfy the criticality criterion (Equation 4) by assessing their dependence on Δt (in multiples of $\langle ISI \rangle$) and the time window w used to evaluate CV .

As shown in Figures C1A and C1B, both for the experimental data and for the subsampled models, $\langle CV \rangle_*$, τ_* , and τ_{t*} decrease with the increase of the time bin Δt , a result which is consistent with those originally obtained by Beggs and Plenz [1]. In Figures C1C and C1D, $\langle CV \rangle_*$, τ_* , and τ_{t*} do not suffer great deviations, being largely

insensitive to w .

Appendix D: CV as a proxy of cortical state

It is known in the neuroscience literature that different levels of spiking variability are related to different cognitive states. In urethane anesthetized brains, there is a slow modulation of the level of synchronization of the ongoing activity. From the experimental perspective, since we cannot ensure stationarity, it is preferable to use the minimum necessary time to calculate CV and define a cortical state. In the literature it is typically arbitrarily accepted to use $w = 10$ s for the estimation of a cortical state. Here we can evaluate, from the model perspective, if this value of w can already provide a good estimation of CV . In Figures D1, we evaluate the standard deviation σ_{CV} of CV as a function of the time used to estimate it. As we can see, a time bin of 20 s provides a better discrimination between the cortical states, saturating the decay the experimental CVs standard deviation. However, despite the fact that a change in w does not impact the results (Figures C1C and C1D), in experiments one needs to compromise between a better statistical definition of CV and not mixing different states due to non-stationarity.

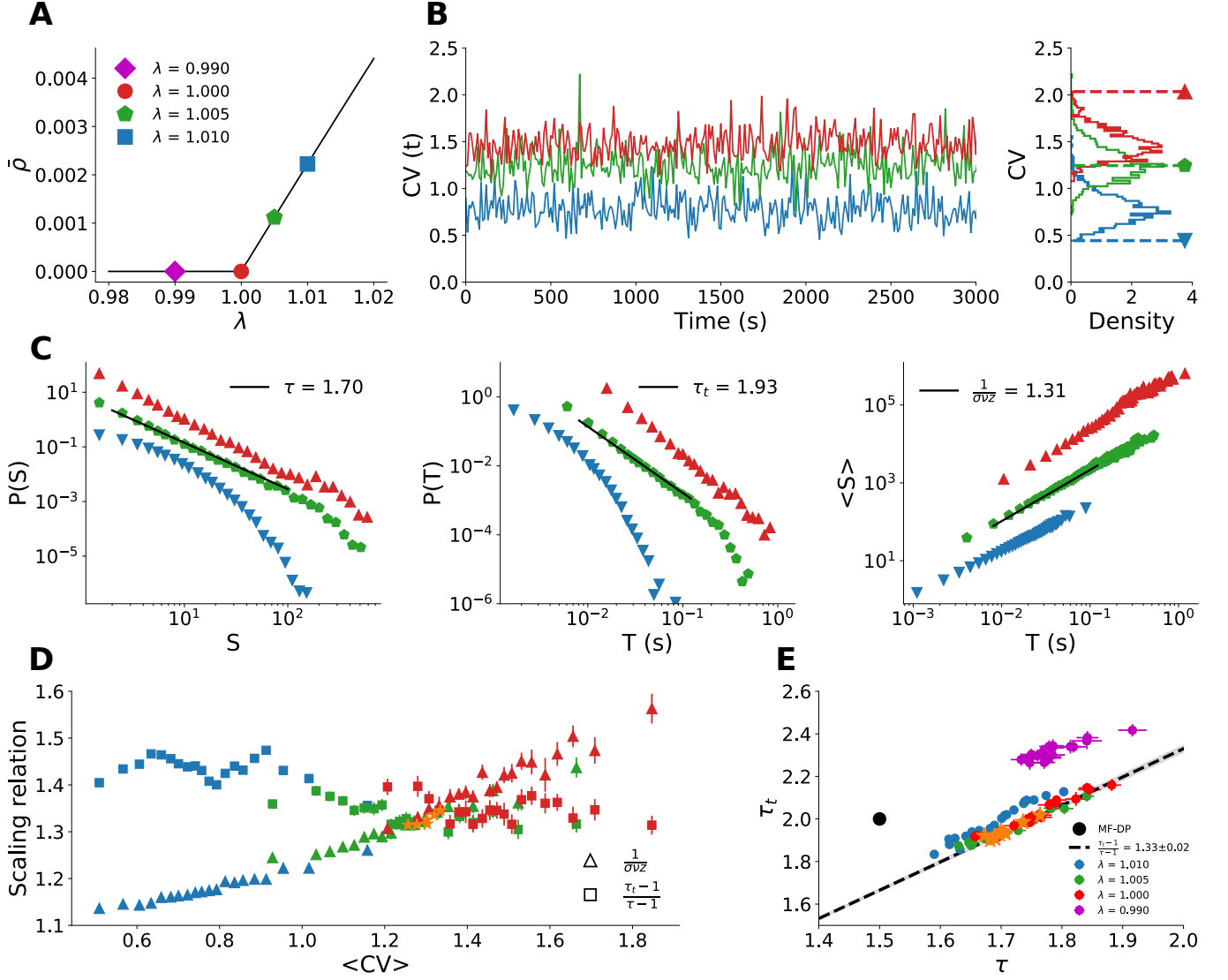


FIG. B1. A probabilistic cellular automaton model with excitation only. **(A)** Stationary density of active sites as a function of the control parameter (branching ratio) λ for the fully sampled model with $N = 10^5$ (see Section II B). Points are simulations and lines are the linear expansion of the mean-field solution. All the remaining plots are for the subsampled model with $n = 500$. **(B)** CV time series and histogram around the critical point $\lambda_c = 1$. **(C)** Exponents τ , τ_t and $1/(\sigma\nu z)$ depend on λ . **(D)** Right- and left-hand sides of the scaling relation Equation (4) coincide around $CV_*^{CA-model} = 1.30 \pm 0.05$. **(e)** Spread of exponents τ and τ_t around the slope $1/(\sigma\nu z)_*^{CA-model} = 1.33 \pm 0.02$.

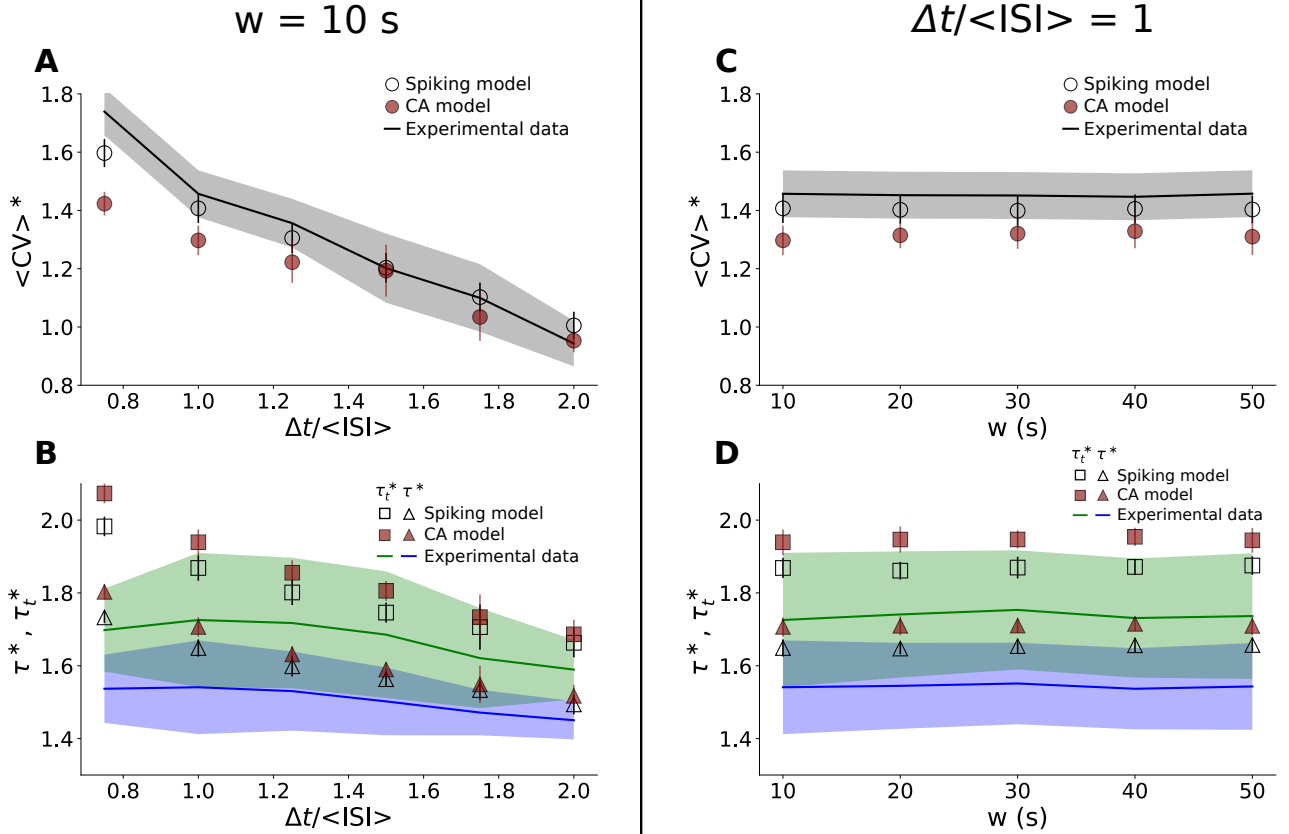


FIG. C1. Dependence of $\langle CV \rangle_*$, τ_* and τ_{t^*} on the temporal windows w and Δt . We compared the group analysis for the experimental data with results for the subsampled models ($n = 100$ for the spiking model and $n = 500$ for the cellular automaton model). For $w = 10$ s, we evaluated (A) $\langle CV \rangle_*$ and (B) τ_* and τ_{t^*} at the point where Equation (4) is satisfied, varying the time bin Δt used to calculate avalanches. Next we fixed $\Delta t = \langle ISI \rangle$ and varied w , the time window to calculate CV , and we evaluated (C) $\langle CV \rangle_*$ and (D) τ_* and τ_{t^*} at the point where Equation (4) is satisfied. We noticed that in all these scenarios, the results from the subsampled models follow the behavior of the experimental data. For the spiking model, g was varied from 1.47 to 1.50 and for the cellular automaton model, λ was varied from 1.00 to 1.01 (for both models, $N = 10^5$). In (C) and (D), we use $NB = \{50, 25, 16, 12, 10\}$ for $w = \{10, 20, 30, 40, 50\}$ s to keep the total sampling time approximately the same (see Methods section in the main paper).

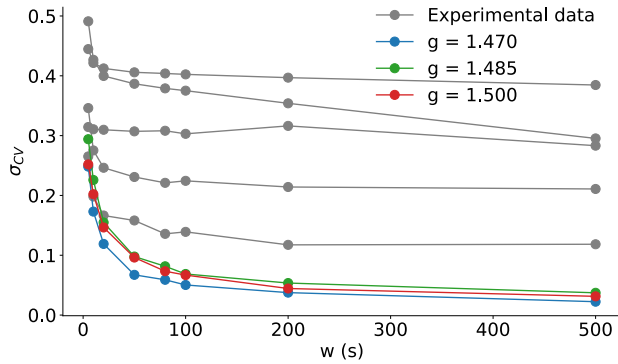


FIG. D1. Dependency of the standard deviation (σ_{CV}) of the CV time series with the time window w used to estimate it. Each gray curve represents the result for each rat studied. The colored curves (see legend) represent values of g of the subsampled spiking model with $n = 100$.